

	S1. Instrumental analysis of washing-up liquid.....	2
	S2. UV-vis. absorption and photolysis	3
10	S2.1 EA proof-of-concept study	3
	S2.2 Results for EB and its derivatives.....	5
	S3. OH radical reaction kinetics	6
	S3.1 PLP-LIF results	7
	S3.2 SAR predictions	8
15	S3.3 Additional material on the photooxidation of EB.....	10
	References	12

20 S1. Instrumental analysis of washing-up liquid

The occurrence of ethyl butyrate (EB) and its derivatives in washing-up liquids was probed by measuring a range of neat Fairy products via headspace extraction and gas chromatography – mass spectrometry (GC-MS) analysis. To prepare the samples, 150 μL of each washing-up liquid were filled into a 20 mL vial without further preparation and measured on the same day. The parameters for the instrumental analysis are listed in Table S1. Compound identification was aided by the NIST mass spectral library. Exemplary chromatograms are shown in Fig. S1.

Table S1: GC-MS parameters for the detection of EB and its derivatives in washing-up liquids.

Parameter	Values
GC, system and column	7890B (Agilent), BPX5
Sample	150 μL in 20 mL vial
Incubation	15 min at 40°C
Injection volume	1500 μL
Inlet temperature	300°C
Split ratio	15:1
Flow rate, carrier gas	1.5 mL min ⁻¹ , Helium
GC oven	Linear temperature ramp (40°C ... 310°C)
Ion source temperature	230°C
MS	7200 Q-TOF (Agilent)

30

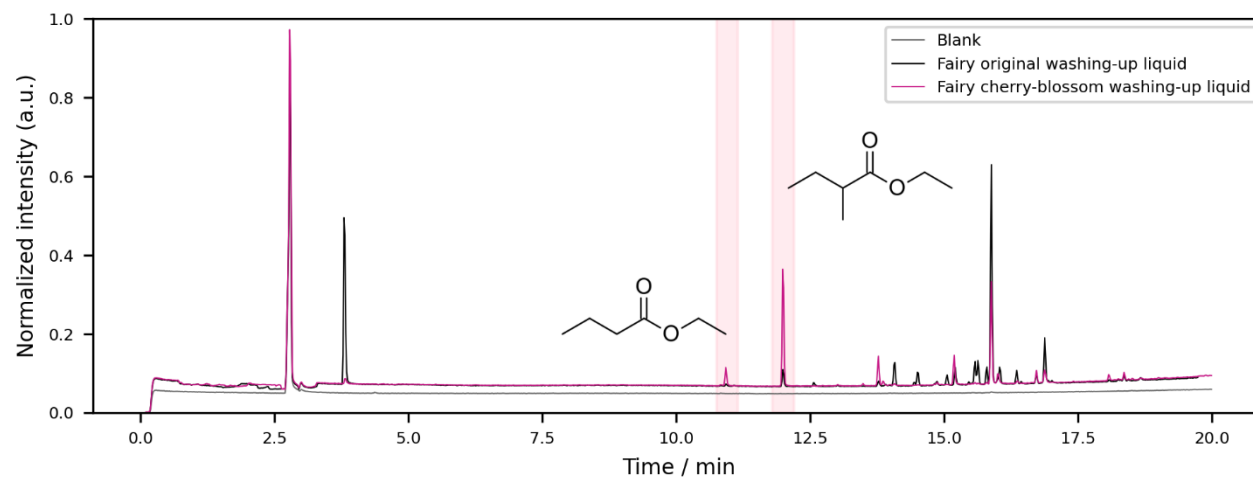


Figure S1: Detection of ethyl butyrate (EB) and ethyl 2-methylbutyrate (EM) in GC-MS headspace samples of Fairy cherry-blossom washing-up liquid.

35 S2. UV-vis. absorption and photolysis

Section S2.1 features a proof-of-concept study which aimed at validating the quasi-gas-phase measurements and deriving a suitable correction factor for ethyl butyrate (EB) and its derivatives by using the same methodology for the structurally related and well-characterized compound ethyl acetate (EA). Section 2.2 includes the experimental and computational results for the UV-vis. absorption of EB and its derivatives. A text file containing the full spectra (of the experimental data) is available as
40 additional material.

S2.1 EA proof-of-concept study

As proof of concept, the solution-phase spectrum of EA recorded in this work is shown alongside the two gas-phase spectra reported in the literature and the spectra calculated by TD-DFT in Fig. S2b, with the values of λ_{max} , ϵ_{max} , and σ_{max} for all spectra
45 listed in Table S2. The two gas-phase spectra from the literature (McMillan, 1966; Śmialek et al., 2016) show excellent agreement in terms of the spectral profile and the intensity, with a clear maximum at around 210 nm. While the TD-DFT calculation predicts a slightly narrower peak profile (hence underestimating absorption intensities between 220 and 250 nm), the peak position and the absorption cross-section at this peak are consistent with the literature spectra. The average \pm standard deviation of λ_{max} and σ_{max} across the three gas-phase spectra are (210.6 ± 0.2) nm and $(1.87 \pm 0.05) \times 10^{-19}$ cm² molec⁻¹. The
50 experimental solution-phase spectrum reproduces the same position of the main absorption peak ($\lambda_{\text{max}} = 211.2$ nm, ± 0.3 nm from the uncertainty of the spectrometer) and agrees very well with the literature gas-phase spectra in terms of the peak width. However, the absorption cross-section is notably higher ($\sigma_{\text{max}} = 2.10 \times 10^{-19}$ cm² molec⁻¹), which is in accordance with previous studies where a change in intensity rather than a shift in wavelength was reported for solution-phase spectra (Mapelli et al., 2023; Nakashima et al., 1982). The solution-phase TD-DFT calculation predicts a slight blue-shift ($\lambda_{\text{max}} = 209.0$ nm) that is
55 not observed in the experimental data, and overestimates the amplification of the absorption cross-section ($\sigma_{\text{max}} = 2.38 \times 10^{-19}$ cm² molec⁻¹). Hence, the solvent effect as predicted by TD-DFT seems to be exaggerated and inaccurate for EA and related molecules with the present choice of functionals and basis sets. These predictions were therefore not performed and evaluated for EB and its derivatives.

60 To obtain a robust measure for accounting for the amplification of the absorption cross-section for spectra recorded in cyclohexane, we integrated the experimental solution-phase spectrum and the literature gas-phase spectra of EA between 200 and 235 nm, and divided the mean area of the two literature spectra by the area of the solution-phase spectrum. This resulted in a correction factor of 0.86 (± 0.01 , from the variability of the two reference spectra), which agrees very well with the work by Mapelli et al. (2023), who have found a factor of 0.93 when comparing the absorption cross-section of butanone to a gas-
65 phase spectrum from the literature. It also agrees with the previous report by Nakashima et al. (1982) of the absorption intensity of solutions prepared in cyclohexane being 1.25 higher (i.e. requiring a correction factor of 0.8) compared to solutions prepared in perfluorohexane which in turn are considered to be realistic quasi-gas-phase samples. While these studies both refer to ketones, the carbonyl groups in esters and aliphatic ketones are reasoned to interact with solvents in comparable ways (Closson and Haug, 1964). The similarity of the derived factor to previously reported factors as well as the very good match between
70 the measured and reported spectra after application of this factor therefore serve to validate the functionality of the spectrometer in the low UV-C range as well as the suitability of cyclohexane as a solvent for short chain esters. Furthermore, wavelength-specific ratios between the spectra show reasonable consistency and agreement with the factor of 0.86 across the absorption band of interest, especially in case of the data by McMillan (1966), confirming the similar peak shape (Fig. S2a). Accordingly, the correction factor was applied to all the experimentally recorded UV spectra in this work.

75

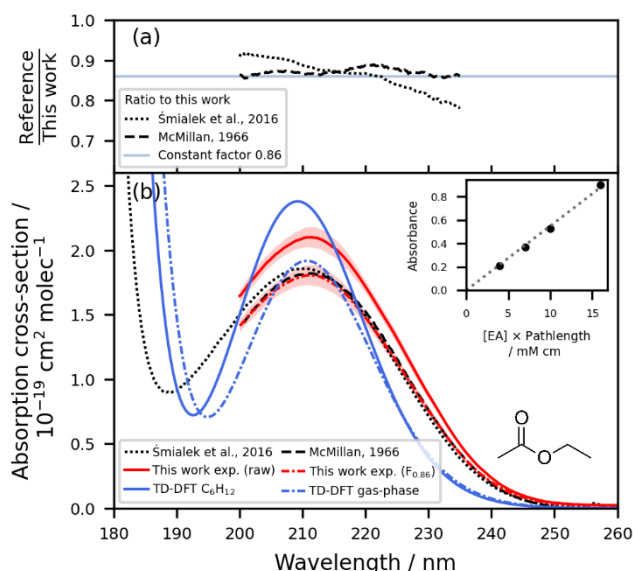


Figure S2: Gas-phase UV absorption of EA. (a) Ratio of the absorption cross-section from each of the two reference gas-phase spectra (McMillan, 1966; Šmialek et al., 2016) to the quasi-gas-phase spectrum from this work, alongside a calculated average factor of 0.86. (b) UV-vis. spectrum of EA. Gas-phase literature spectra from McMillan (1966) and Šmialek et al. (2016) are shown in black. The quasi-gas-phase spectrum from this work (0.004 M - 0.016 M in cyclohexane, $n=4$ excl. blanks, 2σ statistical errors) is shown in red with and without a correction factor of 0.86 to account for the difference between gas-phase and solution-phase absorption. The inset shows an exemplary regression used to derive the molar extinction coefficient via the Beer Lambert law (shown here for the peak wavelength at 211.2 nm), where the uncertainty was derived as the standard error of the slope. Spectra predicted by TD-DFT were calculated at the CAM-B3LYP/6-311++G(d,p) level of theory (30 singlet states), with and without inclusion of cyclohexane as a solvent (CPCM method), and are shown in blue.

Table S2: Absorption maxima and corresponding wavelengths of the $\pi^* \leftarrow n$ transition of EA.

Spectrum	Phase	$\lambda_{\text{max}} / \text{nm}$	$\epsilon_{\text{max}} / \text{M}^{-1} \text{cm}^{-1}$	$\sigma_{\text{max}} / \text{cm}^2 \text{molec}^{-1}$
(Šmialek et al., 2016)	Gas	210.5	48.6	1.86×10^{-19}
(McMillan, 1966)	Gas	210.8	47.6	1.82×10^{-19}
This work (raw)	Solution	211.2	54.9	2.10×10^{-19}
This work ($F_{0.86}$)	(Quasi-)Gas	211.2	47.2	1.81×10^{-19}
TD-DFT gas-phase	Gas	210.5	50.2	1.92×10^{-19}
TD-DFT C_6H_{12}	Solution	209.0	62.2	2.38×10^{-19}

S2.2 Results for EB and its derivatives

The absorption maxima and corresponding wavelengths for the $\pi^*\leftarrow n$ absorption bands of ethyl butyrate (EB), ethyl 2-methylbutyrate (EM), ethyl isovalerate (EI), and isopropyl butyrate (IB) as obtained by experimental and computational approaches are listed in Table S3. Figure S3 shows the entire recorded spectrum for EB, including the near-UV and part of the visible range.

Table S3: Absorption maxima and corresponding wavelengths of the $\pi^*\leftarrow n$ transition of the studied esters according to the experimental data (after accounting for the difference between gas-phase and quasi-gas-phase/solution-phase) and according to the TD-DFT gas-phase predictions. The calculated ratio is the ratio of the experimental σ_{\max} to the σ_{\max} predicted by TD-DFT.

Compound	Experimental			TD-DFT gas-phase			σ_{\max} ratio (exp : TD-DFT)
	λ_{\max} /	ϵ_{\max} /	σ_{\max} /	λ_{\max} /	ϵ_{\max} /	σ_{\max} /	
	nm	M ⁻¹ cm ⁻¹	cm ² molec ⁻¹	nm	M ⁻¹ cm ⁻¹	cm ² molec ⁻¹	
EB	212.0	53.3	2.04×10 ⁻¹⁹	209.5	23.3	0.89×10 ⁻¹⁹	2.3
EM	214.0	76.8	2.94×10 ⁻¹⁹	212.3	57.2	2.19×10 ⁻¹⁹	1.3
EI	213.2	60.0	2.29×10 ⁻¹⁹	210.5	26.8	1.02×10 ⁻¹⁹	2.2
IB	213.0	56.1	2.14×10 ⁻¹⁹	209.3	20.1	0.77×10 ⁻¹⁹	2.8

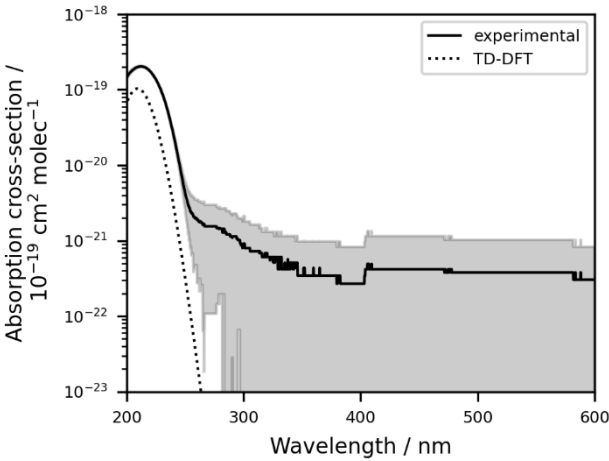


Figure S3: Gas-phase absorption of EB in the UV and visible range, as predicted by TD-DFT and as determined experimentally (after accounting for the difference between gas-phase and quasi-gas-phase/solution-phase).

S3. OH radical reaction kinetics

In the following, supporting information on the kinetics of ethyl butyrate (EB), ethyl 2-methylbutyrate (EM), ethyl isovalerate (EI), and isopropyl butyrate (IB) is presented. The conditions and resulting rate coefficients for all PLP-LIF experiments conducted in this work are listed in Table S4 in Sect. 3.1. Section 3.2 contains predictions by different structure-activity relationships (SARs). Further material on EB is provided in Sect. 3.3, containing a comparison of OH and OD kinetics, an evaluation of O₂ dependence, and the predicted mechanisms and products.

S3.1 PLP-LIF results

Table S4: Absolute values of $k(T)$ for the reactions of EB, EM, EI, and IB with OH radicals determined via PLP-LIF in this work. The number of experiments (n) and the VOC concentration range are given (excluding blanks). If applicable, added oxygen (O_2) is specified. The bath gas was nitrogen for all experiments in York and argon for all experiments in Leeds. Unless stated otherwise, the uncertainties of the rate coefficients were calculated as the 2σ error of the slope of the linear regression of the pseudo first order rate constant k' against [VOC] (see for example Fig. 3 in the main text). In a few experiments (§), the VOC concentration was kept constant while the O_2 concentration was varied, and rate coefficients were determined as the average ± 2 standard deviations of several single-point, offset-corrected calculations of k (k' divided by [VOC]).

Reaction	T / K	p / Torr	n	[VOC] / molec cm^{-3}	[O_2] / molec cm^{-3}	$k / 10^{-12} \text{ molec}^{-1} \text{ cm}^3 \text{ s}^{-1}$	Exp. system
EB + OH	298	29	7	$1.16 \times 10^{14} - 7.83 \times 10^{14}$	No added O_2	5.8 ± 0.6	York
	298	26	6	$4.46 \times 10^{14} - 1.18 \times 10^{15}$	No added O_2	5.4 ± 0.4	York
	314	31	6	$1.73 \times 10^{14} - 1.17 \times 10^{15}$	No added O_2	5.1 ± 0.7	York
	340	31	9	$1.66 \times 10^{14} - 1.44 \times 10^{15}$	No added O_2	5.1 ± 0.3	York
	373	37	8	$2.08 \times 10^{14} - 1.80 \times 10^{15}$	No added O_2	4.9 ± 0.2	York
	407	22	9	$9.46 \times 10^{13} - 9.56 \times 10^{14}$	No added O_2	4.6 ± 0.4	York
	296	37	6	$5.46 \times 10^{13} - 4.56 \times 10^{14}$	No added O_2	5.0 ± 0.4	Leeds
	302	38	10	$6.53 \times 10^{13} - 8.22 \times 10^{14}$	No added O_2	5.6 ± 0.2	Leeds
	477	38	9	3.19×10^{14}	None – 1.44×10^{16}	$5.6 \pm 0.4^\ddagger$	Leeds
	477	6	9	2.31×10^{14}	None – 1.02×10^{16}	$5.0 \pm 0.2^\ddagger$	Leeds
	549	38	6	$3.57 \times 10^{13} - 2.97 \times 10^{14}$	2.86×10^{14}	5.5 ± 0.2	Leeds
	597	37	7	$2.75 \times 10^{13} - 2.28 \times 10^{14}$	None or 3.68×10^{14}	6.7 ± 0.3	Leeds
	740	37	7	$2.17 \times 10^{13} - 1.53 \times 10^{14}$	None or 2.98×10^{14}	10.6 ± 0.5	Leeds
	741	38	8	2.06×10^{14}	None – 9.28×10^{15}	$10.6 \pm 0.9^\ddagger$	Leeds
EB + OD	296	37	5	$1.37 \times 10^{14} - 4.56 \times 10^{14}$	No added O_2	5.8 ± 0.8	Leeds
	597	37	7	$2.75 \times 10^{13} - 2.28 \times 10^{14}$	None or 3.68×10^{14}	6.7 ± 0.5	Leeds
EM + OH	298	35	5	$8.71 \times 10^{13} - 4.22 \times 10^{14}$	No added O_2	6.6 ± 0.7	York
	298	29	7	$2.19 \times 10^{14} - 8.61 \times 10^{14}$	No added O_2	7.2 ± 0.4	York
	314	29	7	$2.08 \times 10^{14} - 8.17 \times 10^{14}$	No added O_2	6.4 ± 0.8	York
	340	31	9	$1.03 \times 10^{14} - 8.92 \times 10^{14}$	No added O_2	5.8 ± 0.4	York
	373	28	7	$1.52 \times 10^{14} - 1.31 \times 10^{15}$	No added O_2	5.5 ± 0.4	York
	402	20	6	$1.12 \times 10^{14} - 4.41 \times 10^{14}$	No added O_2	6.2 ± 0.4	York
EI + OH	298	33	5	$7.93 \times 10^{13} - 3.84 \times 10^{14}$	No added O_2	11.4 ± 0.6	York
	298	24	6	$1.76 \times 10^{14} - 6.90 \times 10^{14}$	No added O_2	11.0 ± 0.6	York
	314	37	6	$1.25 \times 10^{14} - 8.44 \times 10^{14}$	No added O_2	9.3 ± 0.7	York
	340	37	7	$1.15 \times 10^{14} - 7.79 \times 10^{14}$	No added O_2	7.5 ± 1.1	York
	377	24	7	$1.39 \times 10^{14} - 5.46 \times 10^{14}$	No added O_2	6.3 ± 0.8	York
	408	22	8	$5.96 \times 10^{13} - 4.59 \times 10^{14}$	No added O_2	5.7 ± 0.7	York
IB + OH	298	28	6	$6.89 \times 10^{13} - 4.00 \times 10^{14}$	No added O_2	7.4 ± 1.5	York
	298	25	7	$1.85 \times 10^{14} - 7.30 \times 10^{14}$	No added O_2	7.5 ± 0.4	York
	314	31	7	$1.10 \times 10^{14} - 7.40 \times 10^{14}$	No added O_2	6.6 ± 0.8	York
	340	23	9	$7.41 \times 10^{13} - 5.87 \times 10^{14}$	No added O_2	5.8 ± 0.4	York
	381	25	7	$1.44 \times 10^{14} - 5.65 \times 10^{14}$	No added O_2	4.6 ± 0.7	York
	417	22	7	$1.16 \times 10^{14} - 4.54 \times 10^{14}$	No added O_2	4.7 ± 0.8	York

S3.2 SAR predictions

Table S5 features the absolute and relative values of the room temperature partial rate coefficients for the reaction with OH at each site for each of the molecules as predicted by the established SAR by Jenkin et al. (2018). Figure S4 shows the temperature dependence of the total rate coefficient for each molecule as predicted by the same SAR as well as by the SAR by Kwok and Atkinson (1995), whereas Fig. S5 shows the temperature dependence of the site-specific reactivities predicted by the Jenkin et al. (2018) SAR.

Table S5: Rate coefficients for the reactions with OH radicals at room temperature according to SAR predictions (Jenkin et al., 2018). The absolute values are given in units of $10^{-12} \text{ molec}^{-1} \text{ cm}^3 \text{ s}^{-1}$. The relative values refer to the proportion of the reactivity of the site to the total reactivity of the compound. The numbering of the sites is visualized in Fig. 1 in the main text.

Site	EB		EM (CH ₃ at site 3)		EI (CH ₃ at site 2)		IB (CH ₃ at site 4)	
	Abs.	Rel.	Abs.	Rel.	Abs.	Rel.	Abs.	Rel.
1 (CH ₃ , acyl side)	0.18	0.04	0.18	0.03	0.18	0.03	0.18	0.03
2 (CH ₂ or CH, acyl side, β carbon)	2.08	0.46	2.08	0.39	4.02	0.60	2.08	0.33
3 (CH ₂ or CH, acyl side, α carbon)	0.42	0.09	0.80	0.15	0.42	0.06	0.42	0.07
4 (CH ₂ or CH, alkoxy side, β carbon)	1.69	0.37	1.69	0.32	1.69	0.25	3.28	0.52
5 (CH ₃ , alkoxy side)	0.18	0.04	0.18	0.03	0.18	0.03	0.18	0.03
6 (substituted CH ₃ group)			0.35	0.07	0.18	0.03	0.18	0.03

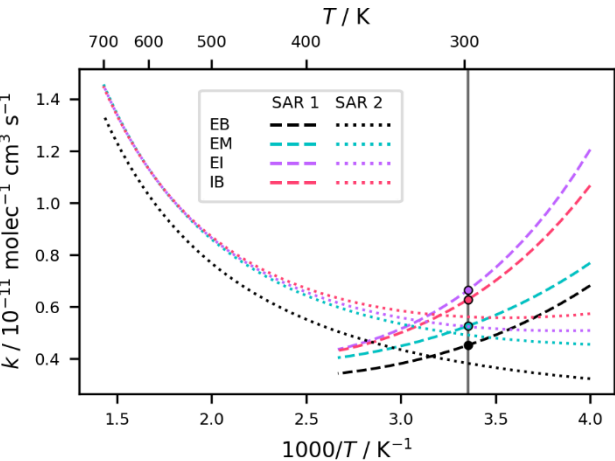


Figure S4: Predictions of the temperature-dependent reactivities of EB and its derivatives according to the SAR by Jenkin et al. (2018) (dashed lines; ‘SAR 1’ in legend) and the SAR by Kwok and Atkinson (1995) (dotted lines; ‘SAR 2’ in legend). The vertical line is $T = 298 \text{ K}$.

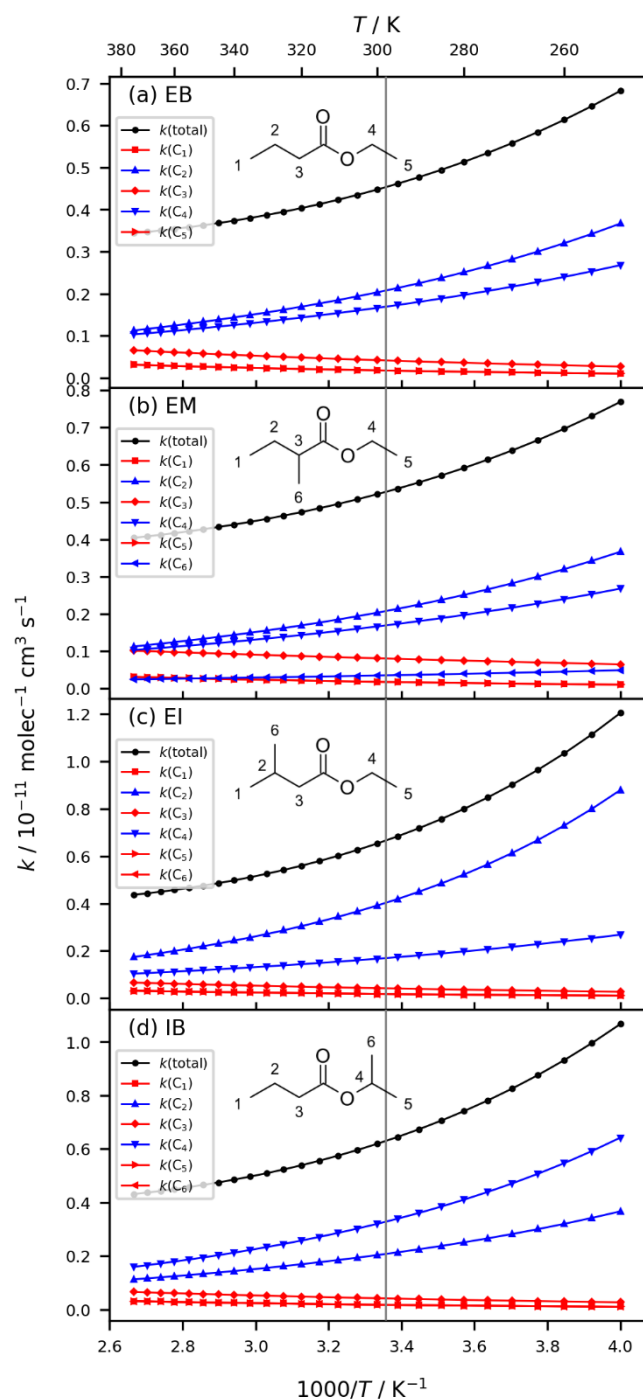


Figure S5: Predictions of the temperature-dependent site-specific reactivities of EB and its derivatives according to the SAR by Jenkin et al. (2018). The overall rate coefficients are shown in black, while the rate coefficients for the individual sites are shown in either blue (negative temperature dependence over shown temperature range) or red (positive temperature dependence over shown temperature range). The vertical line is $T = 298 \text{ K}$.

S3.3 Additional material on the photooxidation of EB

A temperature-dependent comparison of the rate coefficients for the reactions of EB with either OH or OD radicals is illustrated in Fig. S6. Figure S7 shows the OH radical decay in the presence of EB for different O₂ concentrations to probe for OH recycling. The first steps following the reaction of EB with OH at its most reactive sites were evaluated using the Generator for Explicit Chemistry and Kinetics of Organics in the Atmosphere, GECKO-A in short (Aumont et al., 2005), and are illustrated in Fig. S8.

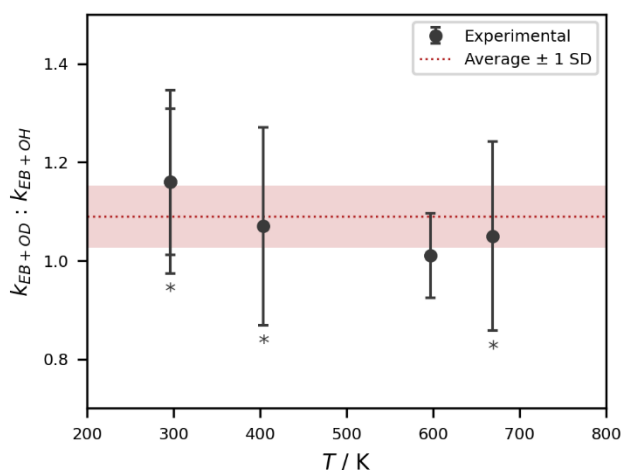


Figure S6: Temperature-dependence of the ratio between k_7 and k_1 . The uncertainties were calculated as the propagation of the errors of the slopes (2σ) of the linear regressions in the bimolecular plots for EB+OD and EB+OH respectively. The value of $k_7:k_1$ at room temperature was measured twice. The * symbol marks experiments that are not listed in Table S4 because EB wasn't delivered accurately enough to determine absolute rate coefficients, but which can be used here because the EB concentration cancels out in the ratio of k_7 to k_1 when following the experimental approach of this study where OH and OD decays were determined in the same cell in immediate succession.

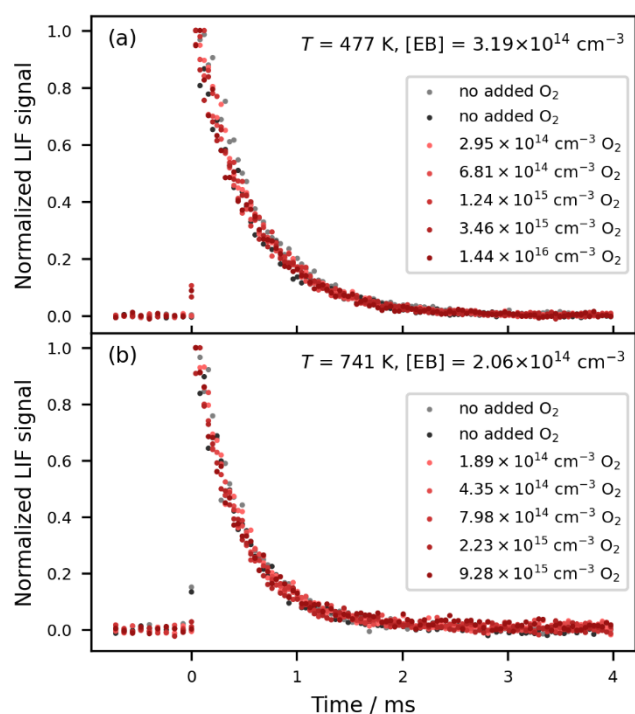


Figure S7: Normalized LIF signal for the decay of OH radicals in the presence of EB at different oxygen (O₂) concentrations at (a) $T = 477$ K and (b) $T = 741$ K, both at $p = 38$ Torr.

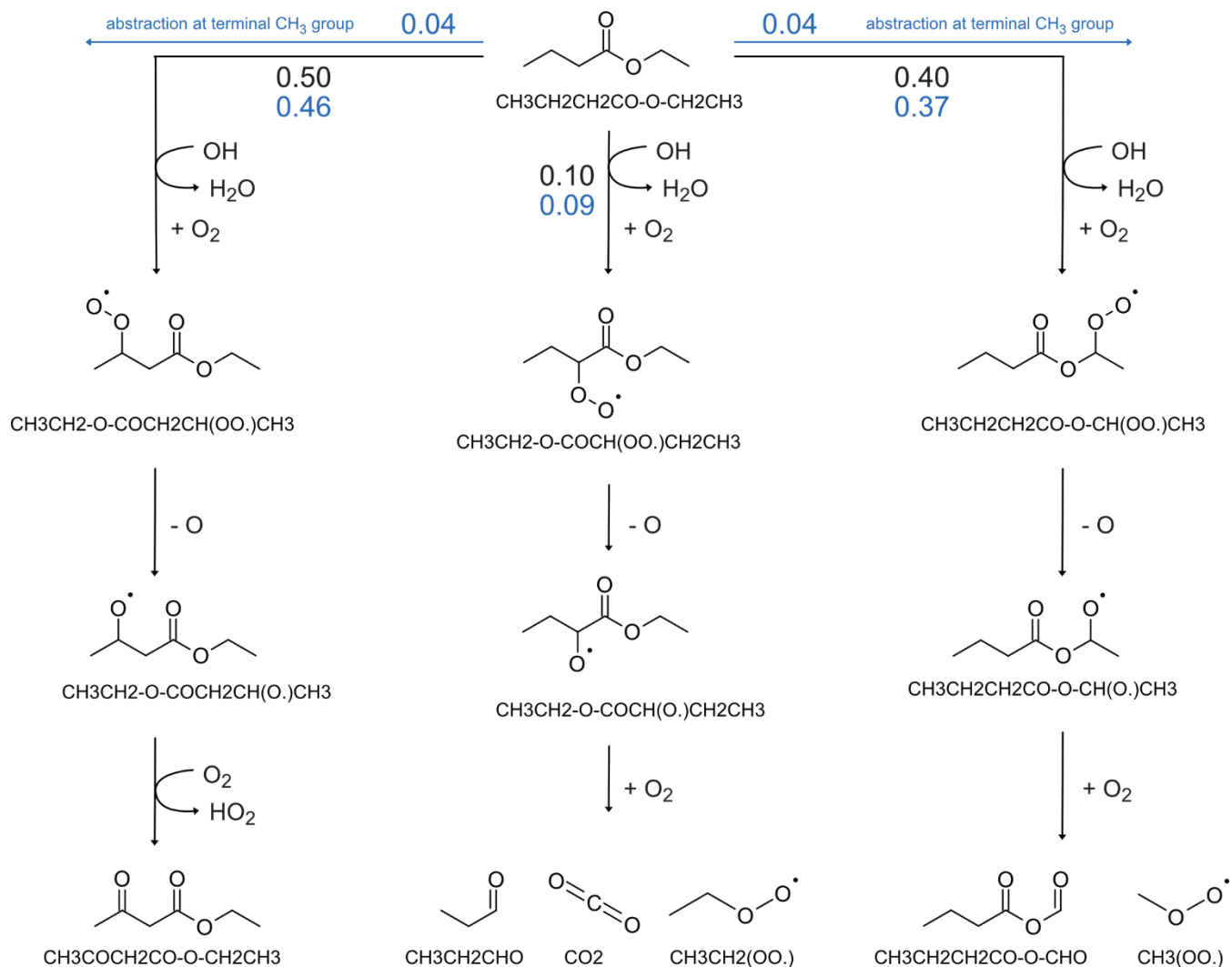


Figure S8: Simplified representation of the main pathways in the OH-initiated photooxidation of EB at sites 2, 3, and 4, as predicted using the Generator for Explicit Chemistry and Kinetics of Organics in the Atmosphere, GECKO-A in short (Aumont et al., 2005). Yields for the initial abstraction at each site are shown in black for the GECKO-A prediction and in blue for the prediction derived from the Jenkin et al. (2018) SAR.

References

- 185 Aumont, B., Szopa, S., and Madronich, S.: Modelling the evolution of organic carbon during its gas-phase tropospheric oxidation: development of an explicit model based on a self generating approach, *Atmospheric Chem. Phys.*, 5, 2497–2517, <https://doi.org/10.5194/acp-5-2497-2005>, 2005.
- Closson, W. D. and Haug, Pat.: The Effects of Solvent and Structure on the Low Intensity ($n \rightarrow \pi^*$) Electronic Transition of Carboxylate Esters, *J. Am. Chem. Soc.*, 86, 2384–2389, <https://doi.org/10.1021/ja01066a018>, 1964.
- 190 Jenkin, M. E., Valorso, R., Aumont, B., Rickard, A. R., and Wallington, T. J.: Estimation of rate coefficients and branching ratios for gas-phase reactions of OH with aliphatic organic compounds for use in automated mechanism construction, *Atmospheric Chem. Phys.*, 18, 9297–9328, <https://doi.org/10.5194/acp-18-9297-2018>, 2018.
- Kwok, E. S. C. and Atkinson, R.: Estimation of hydroxyl radical reaction rate constants for gas-phase organic compounds using a structure-reactivity relationship: An update, *Atmos. Environ.*, 29, 1685–1695, [https://doi.org/10.1016/1352-2310\(95\)00069-B](https://doi.org/10.1016/1352-2310(95)00069-B), 1995.
- 195 Mapelli, C., Donnelly, J. K., Hogan, Ú. E., Rickard, A. R., Robinson, A. T., Byrne, F., McElroy, C. R., Curchod, B. F. E., Hollas, D., and Dillon, T. J.: Atmospheric oxidation of new “green” solvents – Part 2: methyl pivalate and pinacolone, *Atmospheric Chem. Phys.*, 23, 7767–7779, <https://doi.org/10.5194/acp-23-7767-2023>, 2023.
- McMillan, V.: UV absorption spectrum of ethyl acetate (Dataset listed in The MPI-Mainz UV/VIS Spectral Atlas of Gaseous Molecules of Atmospheric Interest as personal communication to J.G. Calvert, J.N. Pitts, Jr. (Photochemistry, John Wiley & Sons, New York, 1966, p. 429)), 1966.
- 200 Nakashima, K., Uchida-Kai, K., Koyanagi, M., and Kanda, Y.: Solvent Effects on the Intensities of Forbidden Bands of Molecules. Absorption Spectra of Acetone and Cyclopentanone, *Bull. Chem. Soc. Jpn.*, 55, 415–419, <https://doi.org/10.1246/bcsj.55.415>, 1982.
- 205 Śmialek, M. A., Łabuda, M., Guthmuller, J., Hubin-Franskin, M.-J., Delwiche, J., Hoffmann, S. V., Jones, N. C., Mason, N. J., and Limão-Vieira, P.: Electronic state spectroscopy by high-resolution vacuum ultraviolet photoabsorption, He(I) photoelectron spectroscopy and ab initio calculations of ethyl acetate, *Eur. Phys. J. D*, 70, 138, <https://doi.org/10.1140/epjd/e2016-70239-9>, 2016.